Supporting information for

Semiconductor Nanocrystals Functionalized with Antimony Telluride Zintl Ions for Nanostructured Thermoelectrics

Maksym V. Kovalenko,[†] Boris Spokoyny,[†] Jong-Soo Lee ,[†] Marcus Scheele,[‡] Andrew Weber,[†] Susanthri Perera,[§] Daniel Landry,[§] Dmitri V. Talapin[†,‡*]*

[†]Department of Chemistry, University of Chicago, IL 60637, USA

[‡] The Molecular Foundry, Lawrence Berkeley National Lab, Berkeley, CA 94720, USA

[§] Evident Technologies Inc., Troy, New York NY 12180, USA

e-mail: mvkovalenko@uchicago.edu, dvtalapin@uchicago.edu

Synthesis of PbTe NCs.

Synthesis of PbTe NCs. A modified recipe by Urban *et al.* was used to synthesize monodisperse PbTe NCs.[1] 10% stock solution of Te in TOP was prepared by slow dissolution of Te shot in TOP at room temperature. In a typical procedure for 5.6 nm PbTe NCs, $Pb(Ac)_3 \times 3H_2O$ (0.569 g, 1.5 mmol), OA (0.7 mL, 2.2 mmol) and squalane (10 mL) were loaded into a 50 mL three-neck flask. The mixture was dried under vacuum at 120 ºC for 1 hour and subsequently heated to 180ºC under nitrogen. 6 mL of TOPTe stock solution were swiftly injected at 180ºC. The reaction mixture was maintained at 155-160 ºC for 3 minutes and cooled to room-temperature using a water bath. PbTe NCs were isolated by adding ethanol to the crude solution followed by centrifugation and re-dissolution in hexane. The ethanol/hexane procedure was repeated 3 more times to purify NCs. Larger NCs can be synthesized by increasing amount of OA (up to 3 mL) and extending the growth time (up to 10 min).[1]

Synthesis of Bi_2S_3 NCs. For a synthesis of 5×25 nm Bi_2S_3 nanorods, a mixture of Bi (III) acetate (0.386 g, 1 mmol), OA (2 mL, ~6.3 mmol) and ODE (20 mL) was heated under vacuum at 110 °C for 1.5 hours. The temperature was then raised to 170 °C under a nitrogen atmosphere. In a separate flask, elemental sulfur (0.32 g, 10 mmol) was dissolved in 10 mL ODE (100 °C, vacuum) to prepare 1 M sulfur stock solution. 2 mL of the sulfur stock solution was then quickly injected into the reaction flask, inducing fast nucleation. After 3 min of growth, the reaction mixture was cooled to room temperature. Nanorods were precipitated by adding hexane (20 mL) and ethanol (5 mL), followed by centrifugation. Two additional steps of dissolution/precipitation using hexane/ethanol as solvent and non-solvent yielded purified Bi_2S_3 nanorods soluble in common solvents such as toluene, chloroform etc. For a synthesis of dot-shaped Bi_2S_3 NCs, a mixture of bismuth (III) acetate (0.772 g, 1 mmol), OA (7 mL, ~22 mmol) and ODE (20 mL) was used while maintaining all other conditions same used for synthesis of Bi_2S_3 nanorods.

Structural and optical characterization. Fourier-transform infrared (FTIR) spectra were acquired in the transmission mode using Nicolet Nexus-670 FTIR spectrometer at resolution of 4 cm^{-1}, averaging over 64 scans. Thick films were deposited on CaF_2 crystal substrates (International Crystal Labs) by drying concentrated NC solutions. IR absorbance was normalized to the weight of absorbing material deposited per unit area. Transmission electron microscopy (TEM) of the samples was carried out using an FEI Tecnai F30 microscope operated at 300kV. For samples prepared from hydrazine solutions, the TEM grids were hydrophilized by a short (5 s) treatment with oxygen plasma prior to NC deposition.

Wide-angle powder X-ray diffraction patterns were collected using a Bruker D8 diffractometer with CuKα X-ray source operating at 40 kV and 40 mA and Vantec 2000 area detector. The initial assignment of crystalline phases was based on the reference files in the Powder Diffraction File (PDF-2) database from International Centre for Diffraction Data (ICDD). The full-profile analysis of powder XRD patterns was conducted using Rietveld refinement method[2,3] (TOPAS software, Bruker). Electrospray ionization mass spectrometry was performed using Agilent 1100 LC/MSD mass-spectrometer. Thermogravimetric analysis was conducted using Shimadzu TGA-50 thermal analyzer at a heating rate of 5 °C/min under a slow nitrogen flow. UV-Vis-NIR absorption spectra were collected using a Cary 5000 spectrophotometer. Thin films were measured using DRA 2500 diffuse reflectance accessory (integrating sphere). Elemental analysis was performed at the Analytical Chemistry Laboratory (ACL) at Argonne National Laboratory using inductively coupled plasma optical emission spectroscopy (ICP-OES). Samples for ICP-OES analysis were prepared by digesting samples in half-concentrated aqua regia.

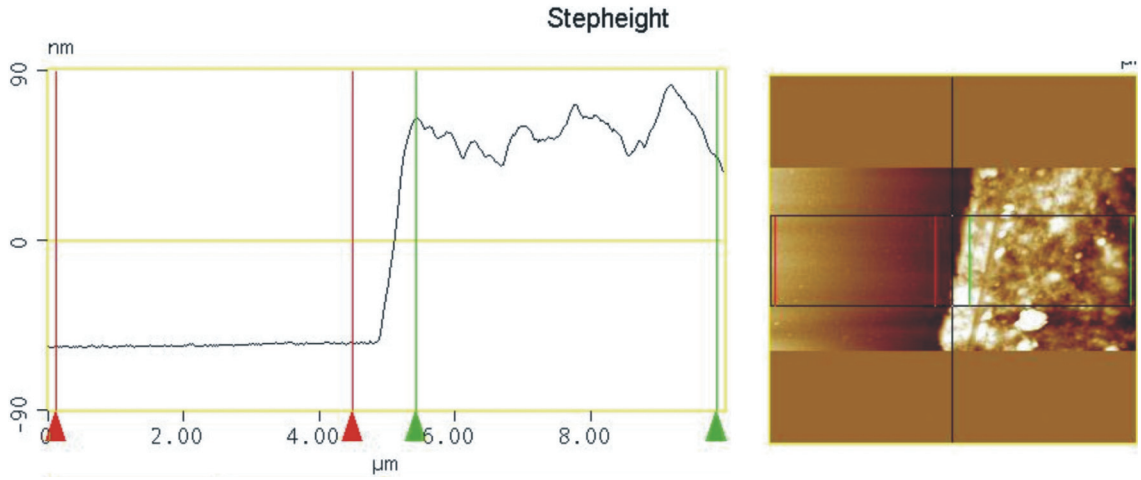

Figure S1. An example of thickness measurements for thin films of thermoelectric materials. AFM image of the scratched area was taken in the tapping mode. The step height is measured as a difference between averaged levels of the film region and substrate level.

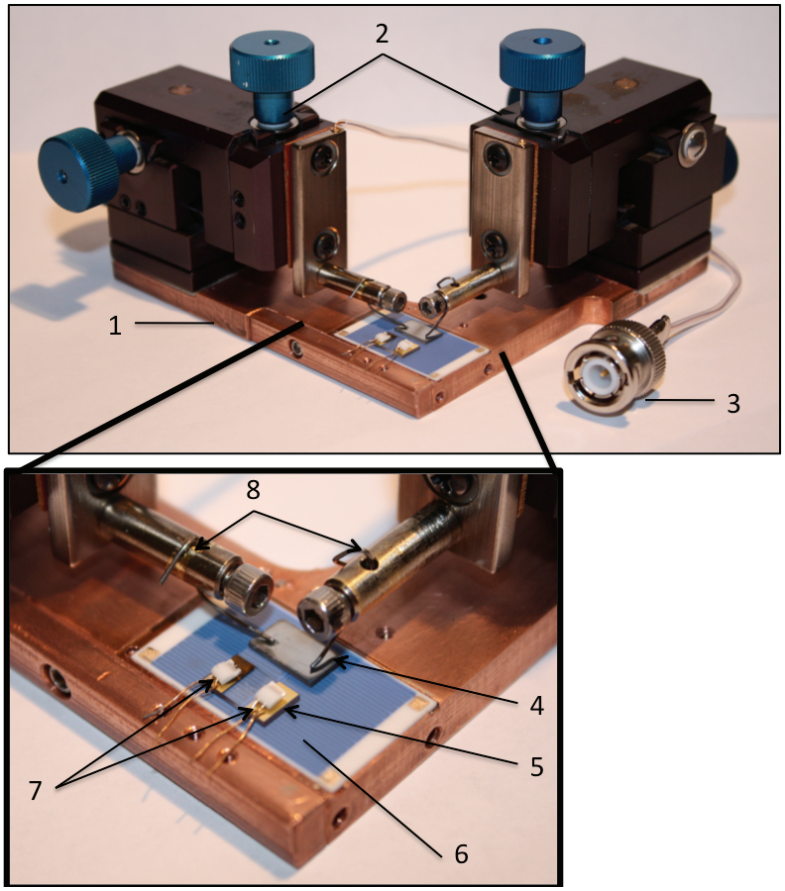

Figure S2. Setup for the measurements of Seebeck coefficient and electrical conductivity of thin-film samples. **1 -** Copper base, **2 –** XYZ Micromanipulators, **3 -** Coaxial cable to voltage probes, **4 -** Test Sample, **5 -** Reference Sample, **6 -** Platinum Heater, **7 –** Omega resistive temperature detectors (RTDs), **8 -** Voltage Probes. For determining Seebeck coefficient, a two sample system was employed, where a blank reference sample **5** identical and symmetrical to that of the test sample **6** was used for measurement of the absolute temperature and supplied temperature gradient using two RTDs **7**. Thermal contact between the RTDs and the reference sample was achieved using an Arctic Silver ceramic thermal compound. A temperature gradient ΔT of 0-20 K was applied across both samples using a platinum heating element **6** (Case Western Univ. Electronic Design), powered by a Keithley 2400 Source Meter. The resulting open circuit voltage, V_{OC} , was measured using two Tungsten probe tips **8**, which were aligned with the test sample electrodes using Miller micromanipulators **2** and adhered using Ted Pella colloidal graphite (for high temperature measurements). For room-temperature measurements, the temperature readings could be obtained by using T-type Omega thermocouples and were the same as with RTDs. Conventional TE heating elements (Custom Thermoelectrics) could also be used to provide temperature gradient for room-temperature measurements. The entire assembly was covered with multiple layers of aluminum foil to ensure uniform temperature distribution across the two sample slides.

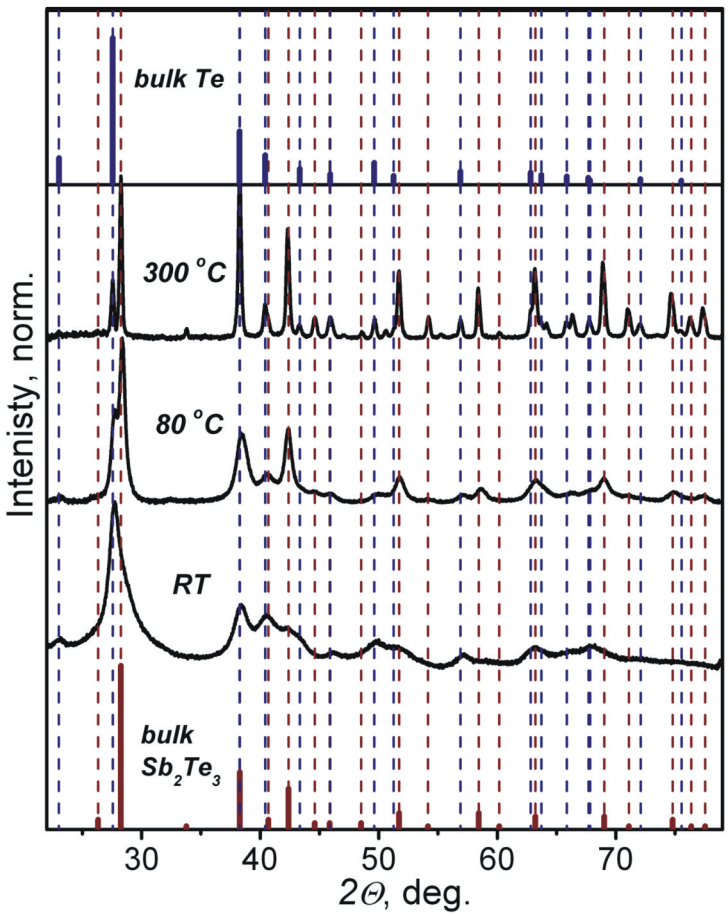

Figure S3. XRD patterns obtained after drying Sb_2Te_3-MCCs at room temperature, and after annealing at 80 ºC and 300 ºC. The decomposition into Sb_2Te_3 and Te is confirmed by comparing diffraction patterns with reference files from the PDF-2 database.

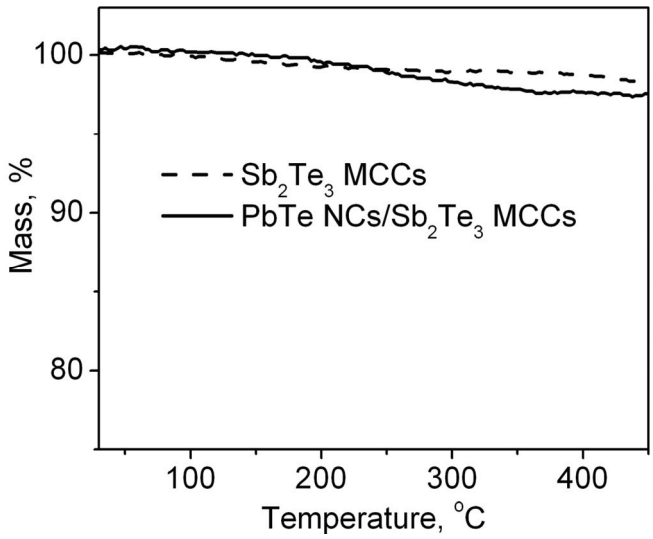

Figure S4. TGA scans for PbTe NCs functionalized with Sb_2Te_3-MCCs (solid line) and for Sb_2Te_3-MCCs (dash line).

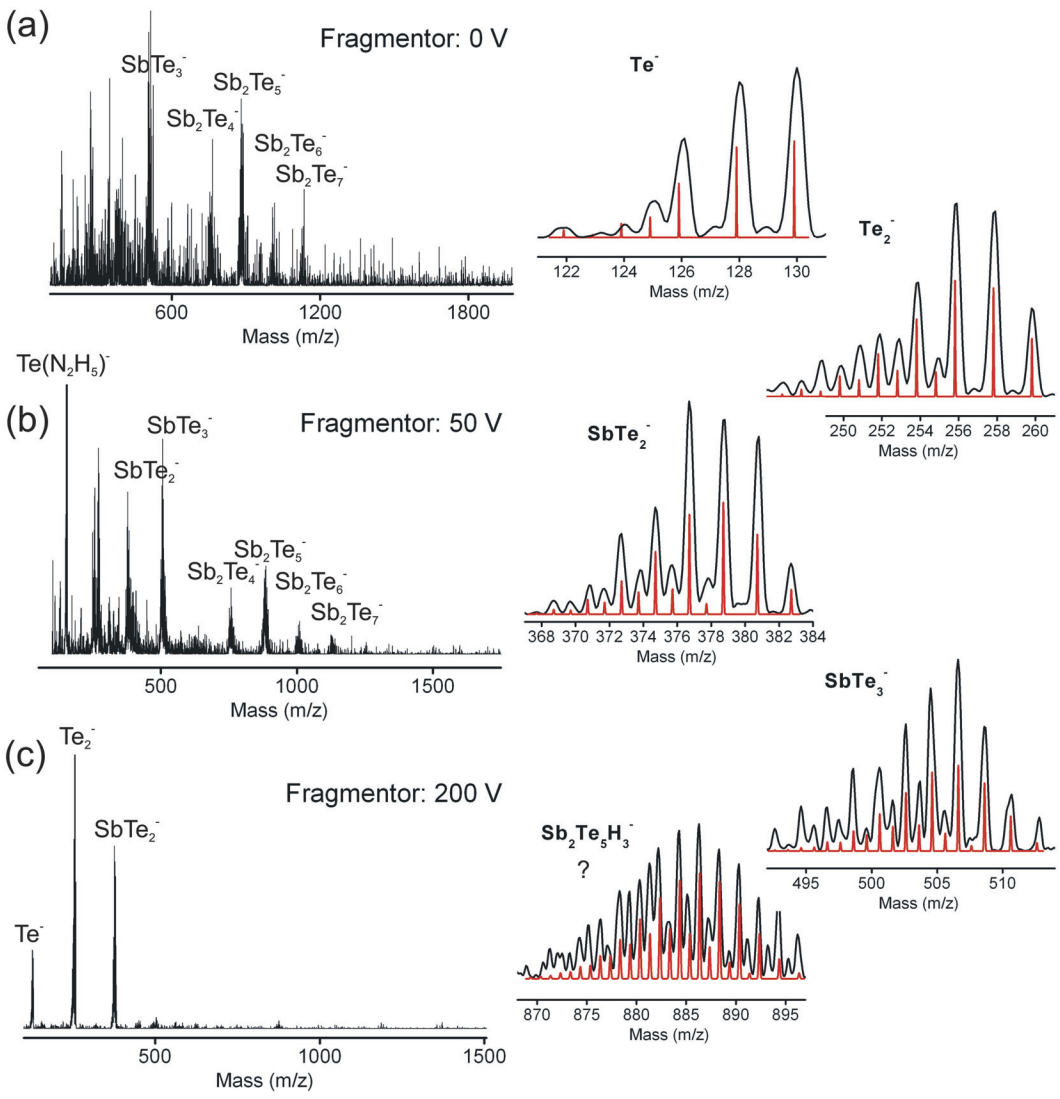

Figure S5. Electrospray ionization mass spectrometry (ESI-MS) of Sb_2Te_3-MCCs in N_2H_4 acquired in negative ion-mode using DMSO as a carrier fluid. As expected, no peaks were observed in positive ion mode. The ESI-MS was chosen as a soft method of mass-spectrometry, which allows analyzing unstable compounds or weakly-bound molecular complexes. The main challenge in the present case was to balance the instability of MCCs with the efficient removal of solvent molecules and counter ions by adjusting the collision induced dissociation at variable collision energies (further referred to as "fragmentor voltage"). The most of information was obtained by comparing the mass-spectra measured at different fragmentor voltages (Figures a, b, and c). At zero votlage, the pattern is overcrowded, especially at small m/z, due to multiple ion-pairs and ion-solvent aggregates. Better resolved peaks obtained at 50 V were assigned to several Sb-Te species based on their m/z values. As can be seen from comparison, most of these ions can be found already at 0V (panel (a)). In agreement with the previous reports for anionic Zintl clusters,[4] the ions appear with reduced charge (-1 for all assigned peaks) due to anion oxidation during the electrospray process. Because of multiple isotopes of Te and Sb with high natural abundances, the assignments based on m/z values can be additionally confirmed by comparing experimental mass-spectra with calculated isotope patterns for each ion (red lines, enlarged spectra on the right side). Thus, perfect matches have been found for Te^-, Te_2^-, $SbTe_2^-$ and $SbTe_3^-$ species. Less

precise matching is observed for larger species (as shown for $Sb_2Te_5^{4-}$), due to the low count rate, high background signal as well as uncertainty due to partial protonation of anions. At a high fragmentor voltage of 200 V, all unstable Sb-Te complexes were decomposed.

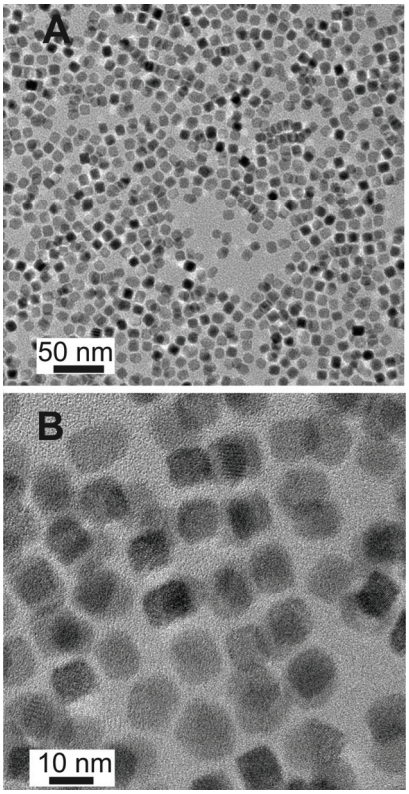

Figure S6. Transmission electron microscopy images for ~10 nm PbTe NCs capped with oleic acid prior to ligand-exchange with Sb_2Te_3-MCCs (compare to Figure 2A).

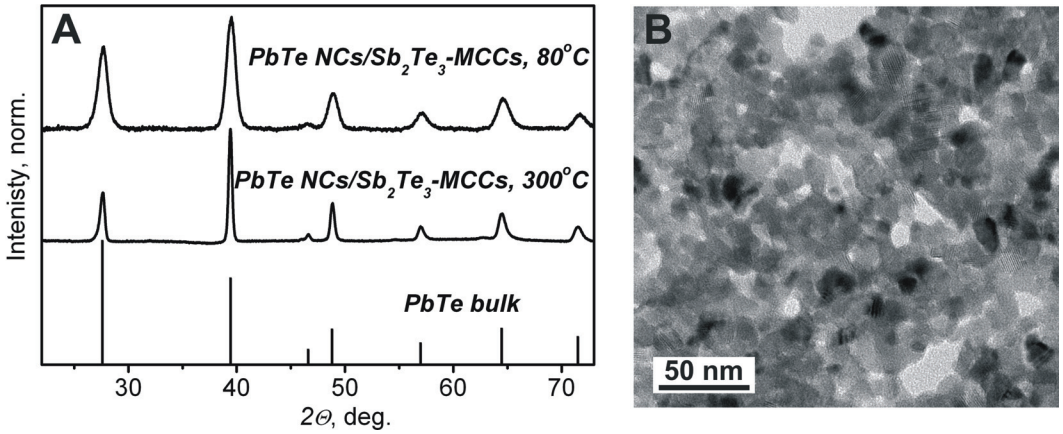

Figure S7. (A) XRD patterns for PbTe NCs capped with Sb_2Te_3-MCCs, annealed at various temperatures. The absence of detectable Sb_2Te_3 peaks points to the very small content of this phase. (B) TEM images for the same sample deposited onto TEM grid and annealed at 300 ^oC.

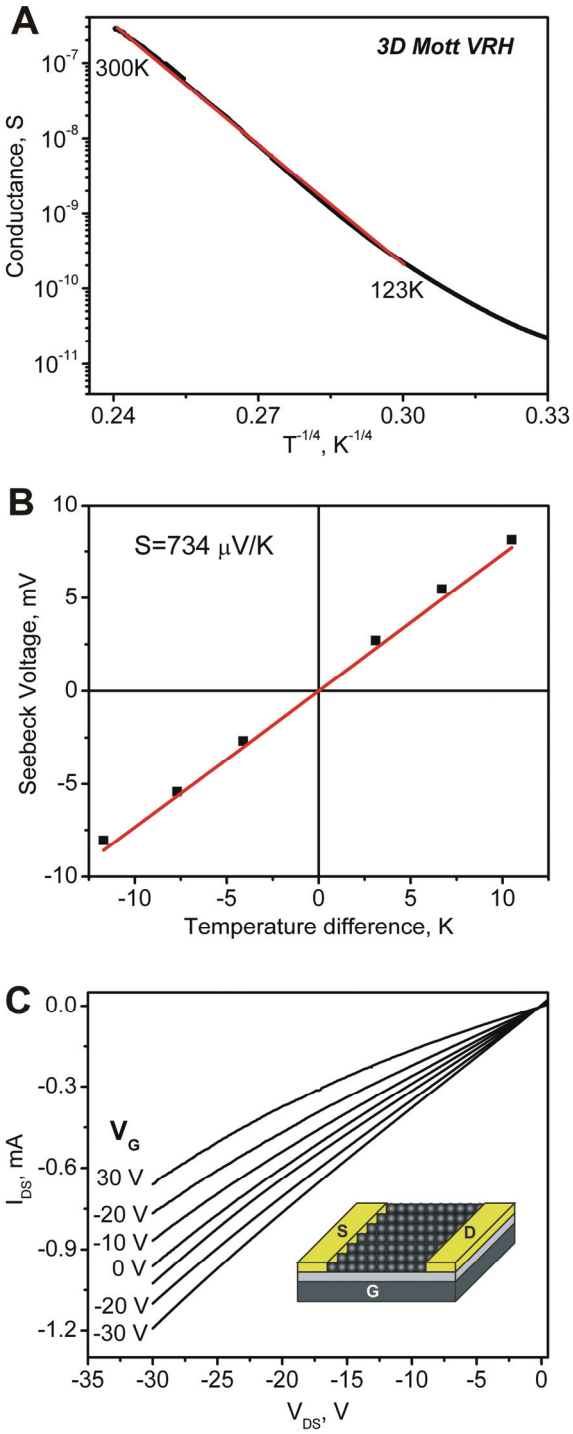

Figure S8. Electrical characterization of PbTe NC solids capped with Sb_2Te_3-MCCs. (A) Plot of the low-field conductance (*G*) vs. $T^{-1/4}$ in the 84-300 K temperature range, (B) Plot of Seebeck voltage vs. temperature difference, (C) Plot of drain current I_{DS} vs. source-drain voltage V_{DS} as a function of gate voltage V_G for a NC-based FET (L=10 μm, W=3800 μm, with a 100-nm thick SiO_2 gate oxide, Au drain and source electrodes, and highly doped Si as the back gate electrode).

Low temperature conductivity measurements were conducted in a four-probe configuration using MPMS (Quantum Design) cryostat for temperature scans. Samples for field-effect transistor

measurements were prepared by depositing very thin films (~17 nm) onto freshly hydrophilized substrates. Even for such thin film it was not possible to achieve the "off" state, e.i. fully deplete the channel, indicative of the high charge-carrier density. Consequently, no gate modulation has been achieved for thicker (50-200 nm) films. This makes it difficult to precisely estimate field-effect mobility, however, a rough estimate from I_D vs. V_G plot gives the hole mobility μ~0.24 cm^2 V^{-1} s^{-1} (Figure S9). With conductivity of 0.05 S cm^{-1}, the hole concentration can be determined from $\sigma=ne\mu$ as n~1.3×10^{18} cm^{-3}.

In the general form, VRH follows G~$\exp(1/T^n)$,[5] where n is determined by sample dimensionality, Coulombic interactions, and the distribution of site energies.[5] In our case, the $\log(G)$ *vs.* $(1/T^n)$ plot is best linearized for n=1/4 (Figure 8A), typical for the three-dimensional Mott-type VRH, in which the hopping electrons find an optimal path with the lowest activation energy and the shortest hopping distance, while the Coulomb interations are small. The presence of Coulomb interaction between sites, the conductivity would scale with temperature with n=1/2 (Efros-Shklovskii VRH), observed, e.g., in CdSe NC solids.[6] The Efros-Shklovskii VRH may be not applicable to arrays of PbTe NCs functionalized with Sb_2Te_3-MCC due to very large dielectric constants (ε) of PbTe and Sb_2Te_3, as the Coulomb interactions become negligible above $T_C = e^4 a g_0 / \left(k_B [4\pi\varepsilon\varepsilon_0]^2\right) < 10K$, where a is the localization length and g_0 is DOS at the Fermi level.[6]

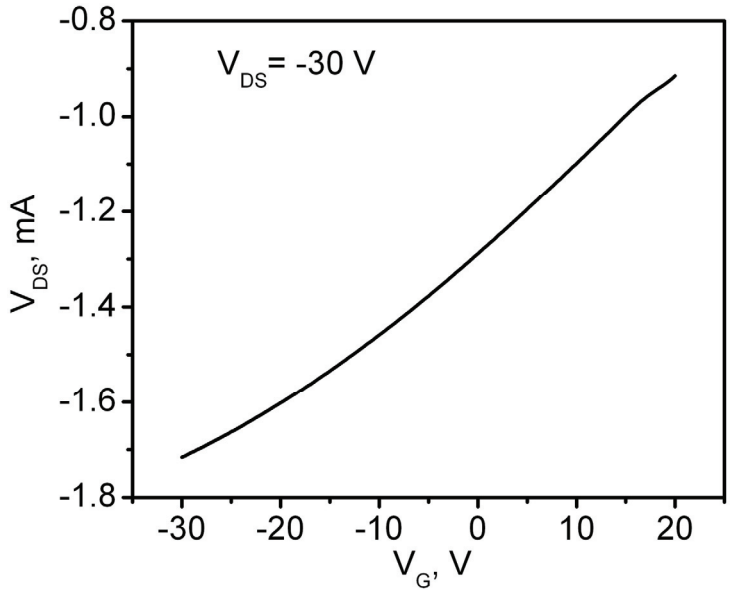

Figure S9. Transfer characteristic (V_{DS} vs. V_G plot) for a field-effect transistor made from PbTe NCs capped with Sb_2Te_3-MCCs (same as shown in Fig. S8C).

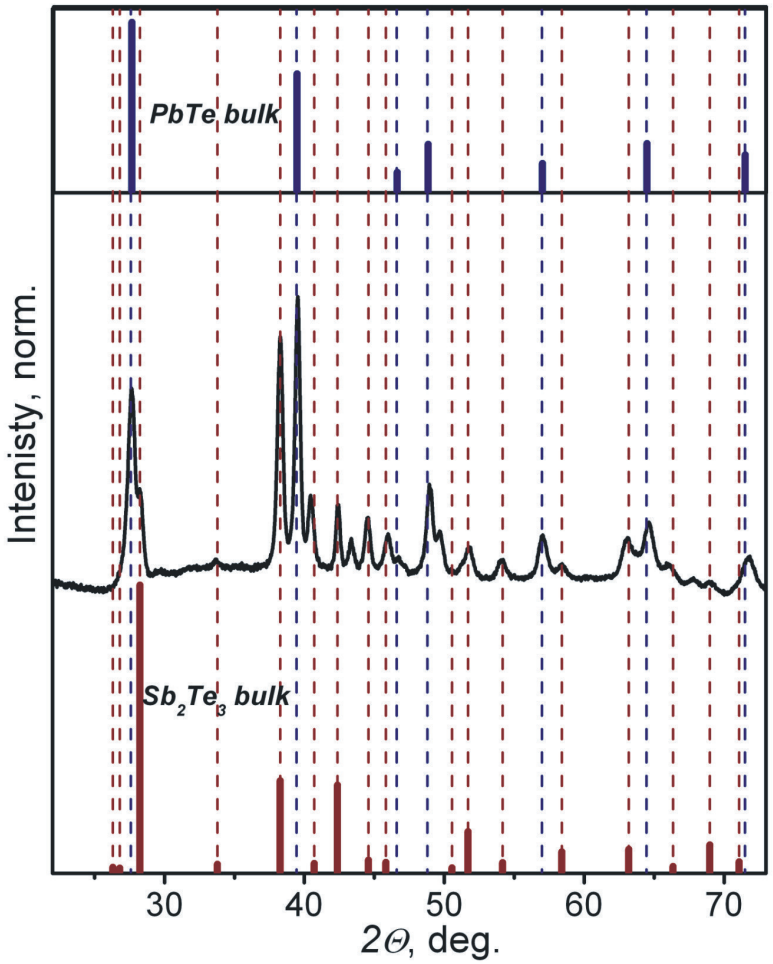

Figure S10. XRD pattern for biphase PbTe/Sb_2Te_3 composite prepared by combining PbS NCs and Sb_2Te_3-MCCs, followed by annealing at 300 ºC.

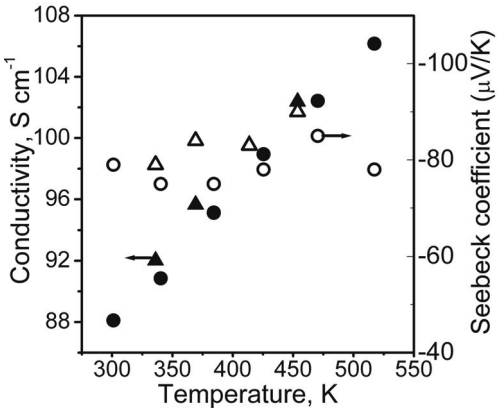

Figure S11. Temperature dependence of electrical conductivity and Seebeck coefficient for the biphase PbTe/Sb_2Te_3 composite deposited by spray-coating in the form of thin films and annealed at 300 ^{o}C. Circles correspond to the forward temperature scan (heating), whereas triangles represent data points measured upon sample cooling.

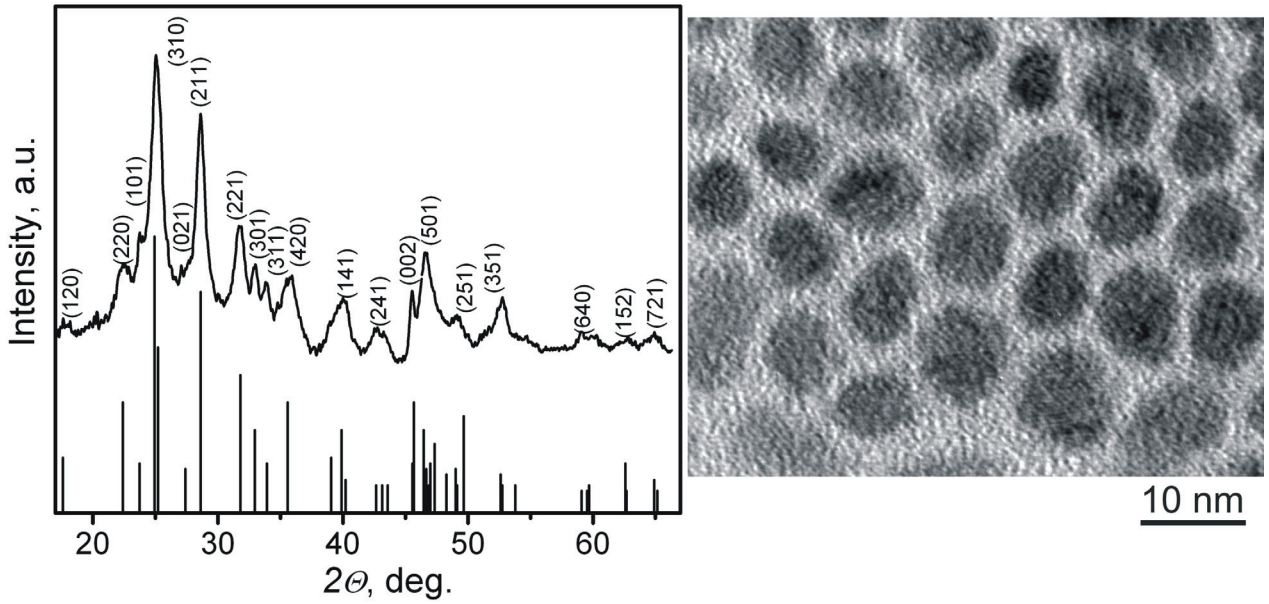

Figure S12. Structural characterization of nearly spherical Bi_2S_3 NCs.

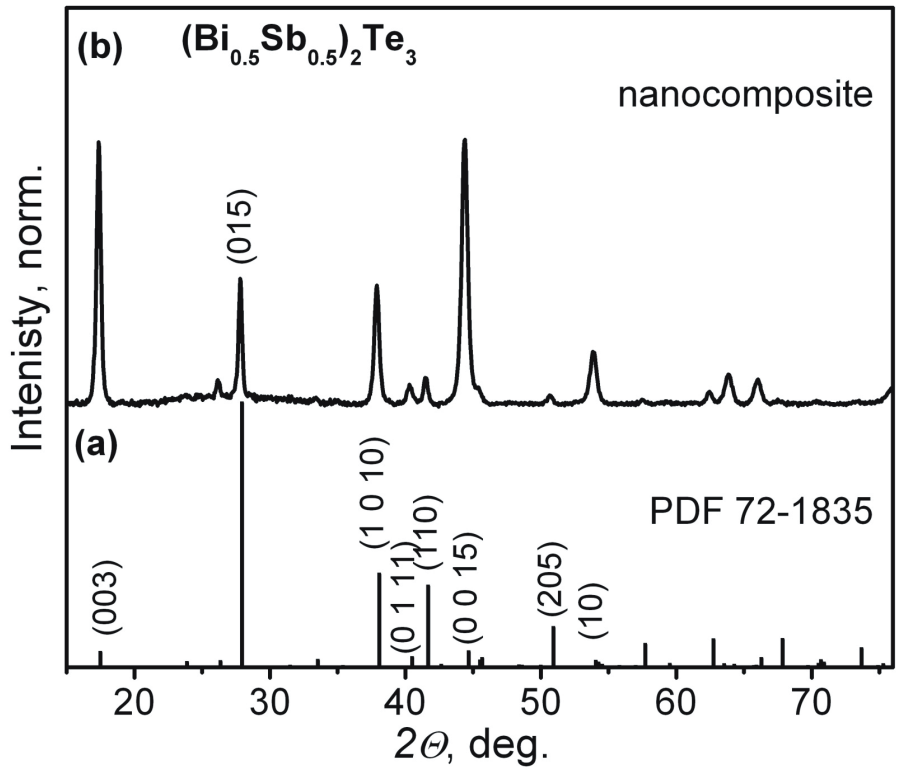

Figure S13. Enlarged XRD pattern and the bulk reflections (PDF-2 database) of $(Bi_{0.5}Sb_{0.5})_2Te_3$ nanocomposite formed through the solid state reaction between Bi_2S_3 nanorods and the Sb-Te precursor. Background from the glass substrate has been subtracted. This is a same pattern as shown in Figure 3C in the Main Text.

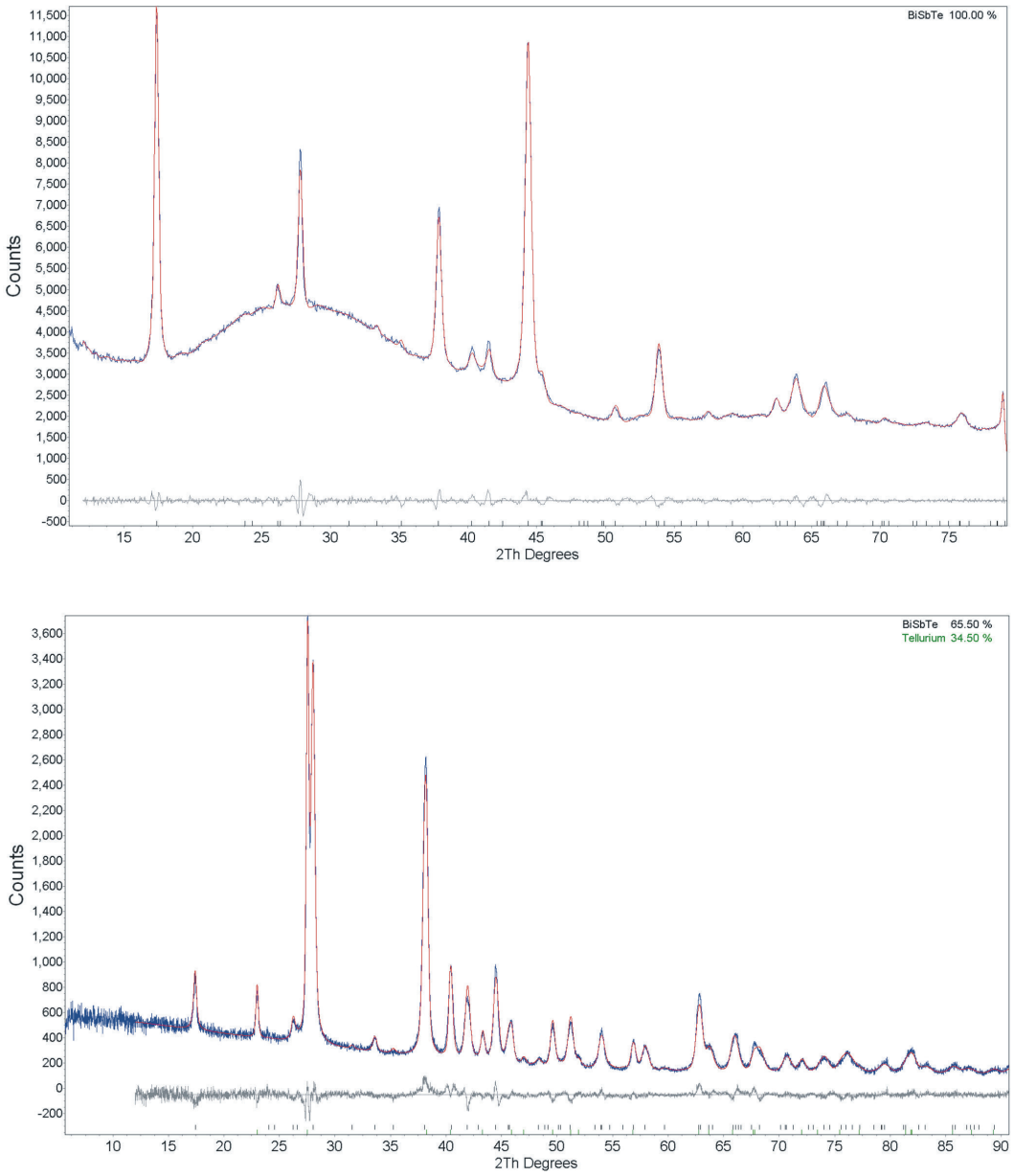

Figure S14. Rietveld refinement for powder XRD patterns: measured XRD patterns (blue), calculated patterns (red) and difference pattern (grey). Figure on top corresponds to $(Bi_{0.5}Sb_{0.5})_2Te_3$ nanocomposite deposited onto glass substrates (Fig. CC, Fig. S13), whereas bottom figure represents $(Bi_{0.12}Sb_{0.88})_2Te_3$ phase containing excess of tellurium prepared in the form of pellet. The amorphous background of glass substrate is seen in the upper panel.

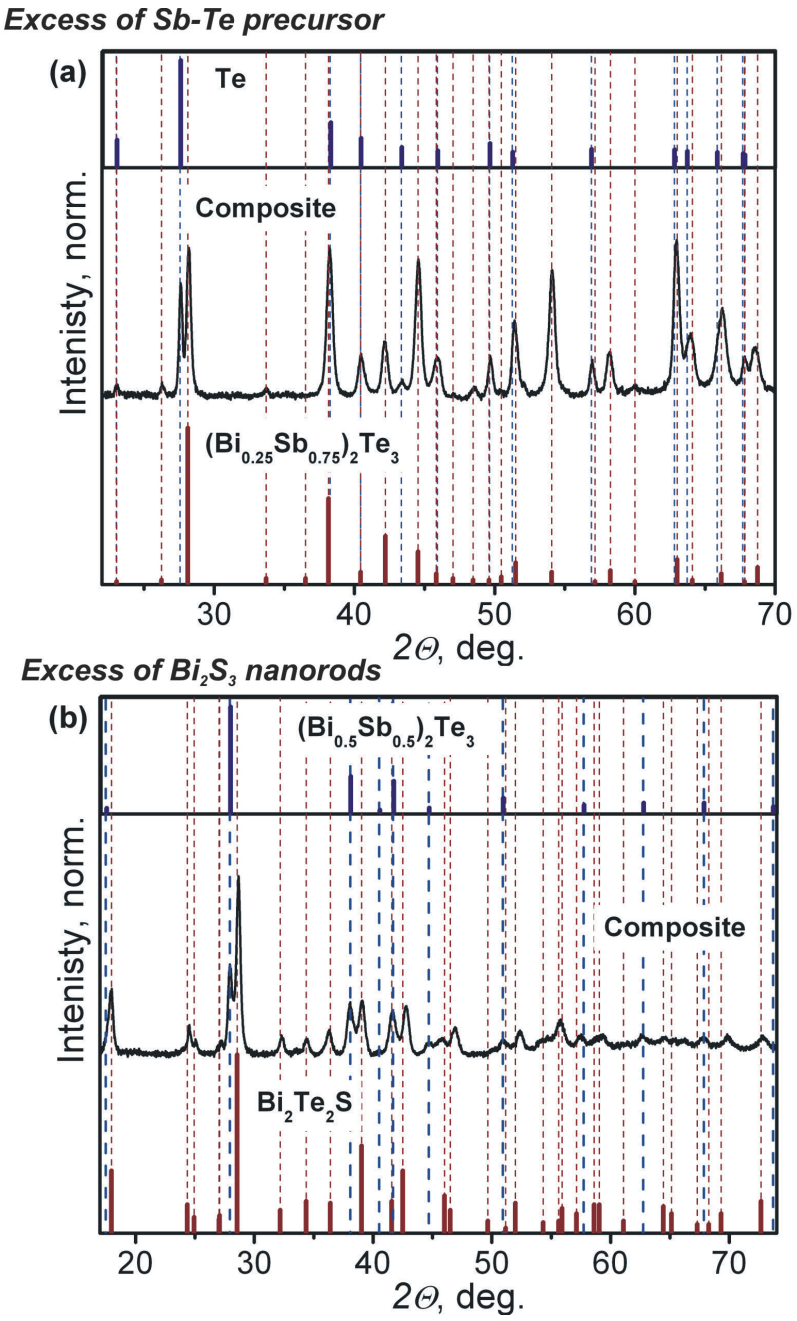

Figure S15. Enlarged XRD pattern along with bulk reflections (PDF-2 database) for $(Bi,Sb)_2Te_3$ nanocomposites formed in the excess of Sb-Te precursor or in the excess of Bi_2S_3.

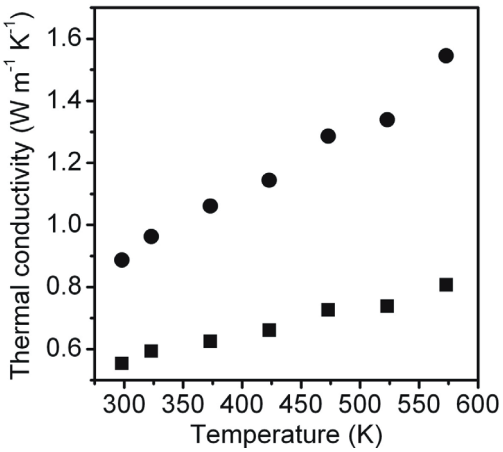

Figure S16. Temperature dependence of thermal conductivity for nanostructured $(Bi,Sb)_2Te_3$ annealed at 350 °C (circles) and 250 °C (squares).

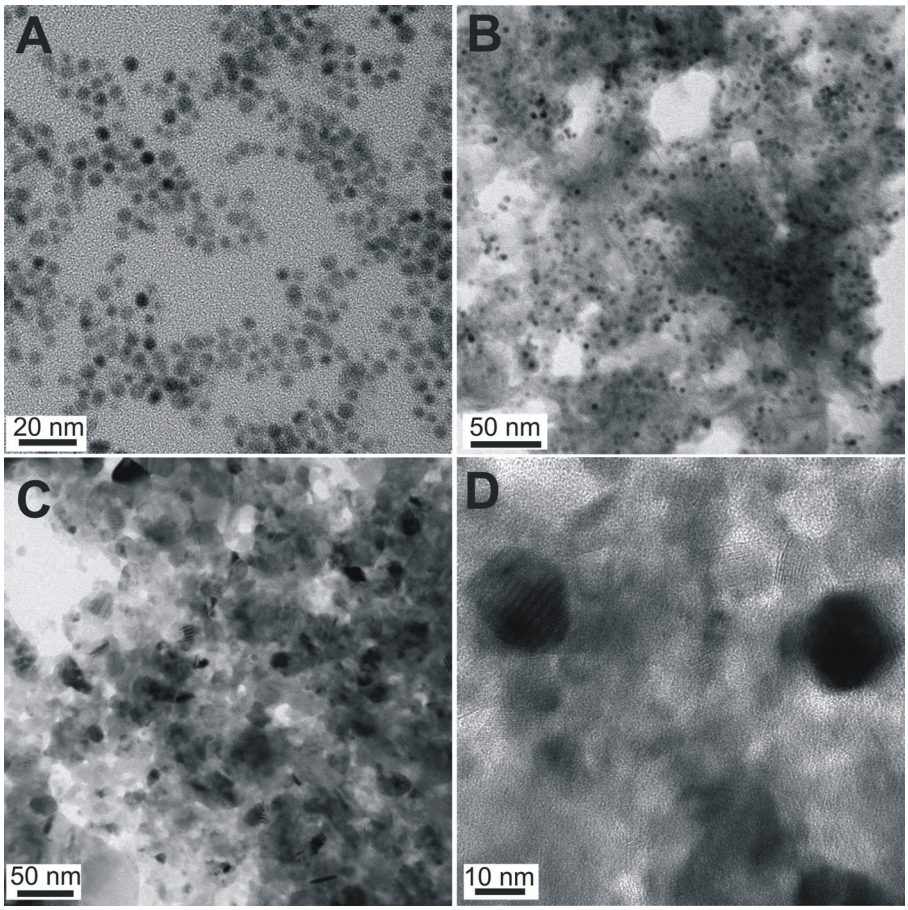

Figure S17. TEM images of (A) 5-nm Au NCs capped with Sb_2Te_3-MCCs, (B) composite prepared by adding Au NCs capped with Sb_2Te_3-MCCs to "BiSbTe ink" (dried at 80 ^oC), showing homogeneous distribution of particles. (C) and (D) Low- and high-resolution TEM images of the same Au/BiSbTe composite annealed at 300 ^oC. Figure (D) illustrated the presence of small and discrete Au inclusions in the annealed sample in addition to large Au precipitates seen from Figure (C).

Supporting references:

(1) Urban, J. J.; Talapin, D. V.; Shevchenko, E. V.; Murray, C. B. *J. Am. Chem. Soc.* **2006**, *128*, 3248-3255.

(2) Rietveld, H. M. *J. Appl. Cryst.* **1969**, *2*, 65-71.

(3) McCusker, L. B.; Von Dreele, R. B.; Cox, D. E.; Louer, D.; Scardi, P. *J. Appl. Cryst.* **1999**, *32*, 36-50.

(4) Goicoechea, J. M.; Sevov, S. C. *Organometallics* **2006**, *25*, 4530-4536.

(5) Mott, N. *Conduction in Non-Crystalline Materials*; 2nd ed.; Clarendon Press Oxford, 1993.

(6) Yu, D.; Wang, C. J.; Wehrenberg, B. L.; Guyot-Sionnest, P. *Phys. Rev. Lett.* **2004**, *92*, 216802